


Controllable Perpendicular Magnetic Anisotropy in Fe/Fe_{100-x}Rh_x Heterostructures Probed by Ferromagnetic Resonance

Hiroki Omura,¹ Sachio Komori^{1,*}, Shigeo Arai,² Kahoru Yoda,² Keiichiro Imura^{1,3} and Tomoyasu Taniyama^{1,†}

¹*Department of Physics, Nagoya University, Furo-cho, Chikusa-ku, Nagoya 464-8602, Japan*

²*Institute of Materials and Systems for Sustainability (IMaSS), Nagoya University, Furo-cho, Chikusa-ku, Nagoya 464-8603, Japan*

³*Institute of Liberal Arts and Sciences, Nagoya University, Nagoya 464-8601, Japan*

 (Received 27 May 2022; revised 4 April 2023; accepted 24 May 2023; published 28 June 2023)

A ferromagnetic-antiferromagnetic (FM-AFM) thin-film heterostructure is proposed to be a potential system that can induce perpendicular magnetic anisotropy (PMA) in a ferromagnet, although there are few material combinations available and the underlying mechanism is not sufficiently understood. Here, we demonstrate that the AFM phase of an Fe-Rh ordered alloy induces PMA in an adjacent Fe layer in an Fe/Fe-Rh heterostructure, which manifests itself as an additional mode of ferromagnetic resonance. The induced interfacial PMA disappears following a magnetic phase transition of Fe-Rh from the AFM to the FM state, suggesting that the AFM order is crucial for the stabilization of PMA. The absence of the additional resonance mode in an Fe/Rh/Fe-Rh control sample suggests that the PMA originates from a magnetic exchange coupling at the Fe/Fe-Rh interface. The results are promising for the development of high-density spintronic devices, in which PMA is controllable through the phase transition of Fe-Rh.

DOI: [10.1103/PhysRevApplied.19.064077](https://doi.org/10.1103/PhysRevApplied.19.064077)

I. INTRODUCTION

A ferromagnet (FM) with large perpendicular magnetic anisotropy (PMA) can provide the basis for nonvolatile spintronic memory devices with high storage density and low power consumption due to reduced stray fields and demagnetizing fields affecting the magnetization dynamics [1,2]. PMA can be developed in a FM near an interface with a heavy metal, where electronic hybridization between $3d$ and $5d$ ($4d$) orbitals induces a change of the magnetic easy axis from in plane to out of plane through a strong interfacial spin-orbit coupling [3,4]. However, in a scheme of current-driven magnetization switching of the FM with PMA for spintronic memory devices, such a strong interfacial spin-orbit coupling, which leads to a large Gilbert damping constant, α , causes an additional energetic drawback, since the critical current density for magnetization switching is proportional to α , raising the long-standing challenge of low-energy magnetization switching [5]. Therefore, numerous efforts have been undertaken to develop PMA heterostructures with relatively small α , such as FM-oxide systems [6–9].

In recent years, an antiferromagnet (AFM)-FM heterostructure has attracted much interest as an alternative system that can realize PMA [10–13]. Since PMA in the

FM-AFM system does not rely on spin-orbit coupling but on exchange coupling, the issue of a large critical current due to strong spin-orbit coupling can be circumvented. Also, a complex multilayer structure is not required to stabilize PMA, and hence, the thickness of the magnetic layer in a magnetic memory device based on the FM-AFM interface can be reduced, which is also favorable for reducing the switching energy. Several studies have suggested that the underlying mechanism of the AFM-induced PMA in a FM is related to a magnetic exchange interaction between an FM layer and unpinned spins induced within an AFM layer at an FM-AFM interface [11,12,14]. Although there are few reports on AFM-induced PMA and the exact mechanism remains an open question, the rich physics associated with the controllability of spin textures in an AFM (e.g., magnetoelectric coupling, magnetoelastic coupling, and a magnetic phase transition) potentially offer alternative forms of PMA devices.

An Fe-Rh ordered alloy is an AFM with such a variety of physics and is promising for spintronic applications. Upon heating, Fe-Rh exhibits a first-order phase transition from the AFM to the FM state at around 360 K [15–18], which is accompanied by an isotropic lattice volume expansion of 1% [17]. The strong coupling between the lattice and the magnetic degrees of freedom in Fe-Rh can lead to controllable FM ordering in an FM/Fe-Rh heterostructure by heat [19–22], strain [23–25], and chemical composition [26–28]. In particular, gate-controllable spin textures in

*komori.sachio.h0@f.mail.nagoya-u.ac.jp

†taniyama.tomo@nagoya-u.jp

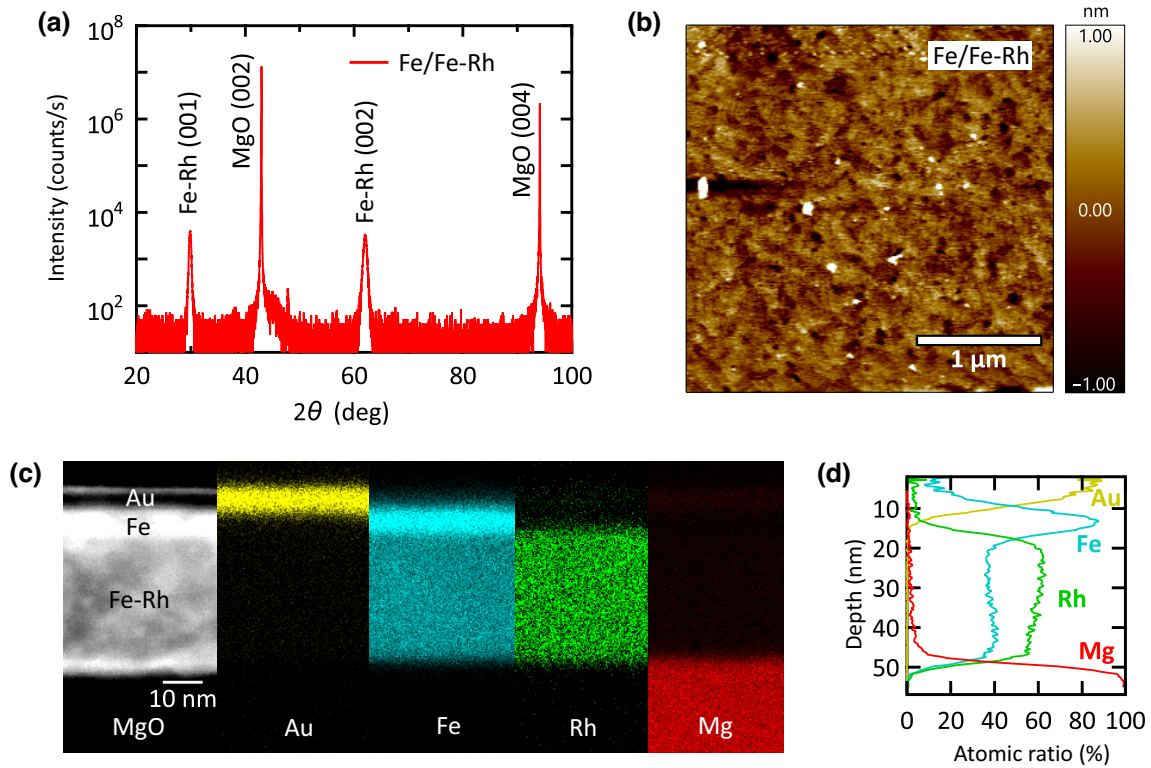


FIG. 1. (a) High-angle x-ray diffraction; (b) atomic-force-microscopy surface image; (c) scanning-transmission-electron micrograph with energy-dispersive x-ray maps for Au (yellow), Fe (cyan), Rh (green), and Mg (red); and (d) depth profiles for Fe(6 nm)/Fe-Rh(32 nm) on a MgO(001) substrate.

Fe-Rh on a ferroelectric material potentially realize voltage control of magnetic anisotropy (VCMA) of an adjacent FM material with PMA, which is promising for energy-efficient magnetization switching. Indeed, VCMA in PMA systems based on carrier doping [29–31], strain transfer [32], and ionic migration [33] have been intensively studied for magnetization switching [29,30] and controlling domain-wall dynamics [34,35], which can be potentially applied to ultralow-power spintronic memory devices [36]. The FM/Fe-Rh heterostructure could realize controllable PMA through the VCMA effect based on a magnetic phase transition.

Here, we report a large interfacial PMA in an Fe/Fe-Rh heterostructure and investigate the effect of the magnetic phase transition. From ferromagnetic resonance (FMR) measurements, we determine a PMA constant of $K_{u\perp} = 8600 \text{ kerg cm}^{-3}$ for an additional FMR mode that emerges when Fe-Rh is in the AFM state. The magnetic phase transition of the Fe-Rh layer from the AFM to the FM state results in a decrease in the PMA down to $K_{u\perp} = 150 \text{ kerg cm}^{-3}$, suggesting that magnetic coupling between the AFM order of the Fe-Rh layer and the FM order of the Fe layer is key to the development of the large PMA.

II. EXPERIMENTS

Heterostructures of Fe(6)/Fe-Rh(32) (thicknesses in nanometer units) with an exchange-coupled Fe/Fe-Rh interface and Fe(6)/Rh(2)/Fe-Rh(32), in which the Rh interlayer blocks the exchange coupling between Fe and Fe-Rh, are fabricated on [001]-oriented MgO substrates by molecular beam epitaxy in an ultrahigh-vacuum chamber with a base pressure better than 1×10^{-9} Torr. The substrate is preannealed at 600 °C for 1 h and Fe-Rh is deposited using separate Fe and Rh sources at the rate of 0.020 nm s^{-1} at 450 °C. The Fe-Rh films are postannealed at 620 °C for 1 h, and Fe and Rh layers are subsequently deposited at room temperature. The films are capped with 4-nm-thick Au. Magnetization of the samples is characterized by vibrating sample magnetometry (VSM). Dynamic magnetic properties are measured with a broadband FMR setup involving a vector network analyzer and a coplanar waveguide. The microwave power absorbed by a sample is measured by sweeping the microwave frequency (f) from 1 to 20 GHz at fixed external in-plane magnetic fields (H) of 0–4000 Oe. H is applied along the [100] direction of Fe-Rh for VSM and FMR measurements.

III. RESULTS AND DISCUSSION

In Fig. 1(a), we plot high-angle x-ray diffraction data from an Fe(6)/Fe-Rh(32) bilayer, which confirm [001] c -axis growth of $B2$ -ordered Fe-Rh on MgO with rocking curves of (001) and (002) Bragg peaks showing full width at half maximum values of 0.31° and 0.26° , respectively. From the relative intensities of the Bragg peaks, the chemical order parameter, S , of $B2$ -ordered Fe-Rh is estimated to be $S = (I_{001}^{\text{expt.}}/I_{002}^{\text{expt.}})^{0.5}/(I_{001}^{\text{calc.}}/I_{002}^{\text{calc.}})^{0.5} = 0.82$, where $I_{001}^{\text{expt.}}$ and $I_{001}^{\text{calc.}}$ are the experimental and theoretically calculated [37,38] peak intensities, respectively. For an Fe(6)/Rh(2)/Fe-Rh(32) trilayer, we estimate $S = 0.90$. The S values obtained here are either comparable to or higher than the values reported for Fe-Rh thin films with comparable thickness grown on MgO substrates [37,39,40], confirming the structural and chemical homogeneity of Fe-Rh in our samples. Diffraction peaks from the 6-nm-thick Fe layer are undetectable, which is likely due to the small grain size of thin Fe. However, an Fe(12)/Fe-Rh(32) control sample with relatively thick Fe deposited under similar conditions shows (002) and (110) diffraction peaks (see Fig. S1 within the Supplemental Material [41]), suggesting the polycrystalline nature of the Fe layer deposited at room temperature. Figure 1(b) shows the atomic force microscopy image on the surface of the Fe(6)/Fe-Rh(32) bilayer, showing an atomically flat surface with a root-mean-square surface roughness of 0.4 nm over an area of $9 \mu\text{m}^2$. Cross-section scanning transmission electron microscopy (STEM) energy-dispersive x-ray (EDX) maps for the Fe(6)/Fe-Rh(32) bilayer in Fig. 1(c) and their depth profile in Fig. 1(d) demonstrate atomically sharp interfaces and rule out intermixing and changes in local composition at the Fe/Fe-Rh interface (see Fig. S2 within Supplemental Material for detailed TEM characterization [41]).

In Fig. 2(a), we plot in-plane magnetization versus magnetic field [$M(H)$] loops at 310 K for the Fe(6)/Fe-Rh(32) bilayer and the Fe(6)/Rh(2)/Fe-Rh(32) trilayer. We note that M is calculated from the total volume of the Fe and Fe-Rh layers. At 310 K, the Fe-Rh layer is in the AFM state, and hence, the magnetic moment is predominated by the ferromagnetism of the Fe layer. The coercive field (H_c) of the Fe(6)/Rh(2)/Fe-Rh(32) trilayer is 20 Oe, which is comparable to the H_c of an Fe(6) single layer on a MgO (001) substrate [see Fig. S3(a) within the Supplemental Material [41]], while the Fe(6)/Fe-Rh(32) bilayer shows a notably large H_c of 220 Oe, indicating that a magnetic exchange coupling at the Fe/Fe-Rh interface leads to an increase in H_c of the Fe layer, consistent with previous reports on Fe/Fe-Rh [21] and NiFe/Fe-Rh [42] grown on MgO (001) substrates. The independent magnetization switching behavior in the $M(H)$ loop of the Fe(6)/Rh(2)/Fe-Rh(32) trilayer results from switching of the Fe layer with a

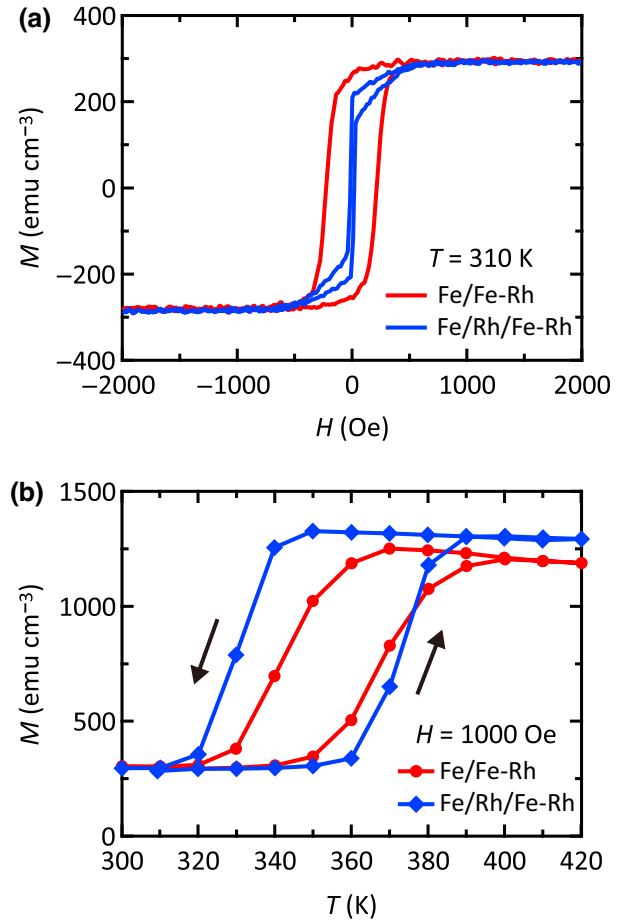


FIG. 2. (a) $M(H)$ loops for Fe(6 nm)/Fe-Rh(32 nm) (red curve) and Fe(6 nm)/Rh(2 nm)/Fe-Rh(32 nm) (blue curve) at 310 K. (b) $M(T)$ curves near the magnetic phase transition of Fe-Rh for Fe(6 nm)/Fe-Rh(32 nm) (red curve) and Fe(6 nm)/Rh(2 nm)/Fe-Rh(32 nm) (blue curve) at $H = 1000$ Oe.

saturation magnetization of $M_s \approx 1500 \text{ emu cm}^{-3}$ [corresponding to $M_s \approx 240 \text{ emu cm}^{-3}$ in Fig. 2(a)] and the residual FM phase with $M_s \approx 30 \text{ emu cm}^{-3}$ [$M_s \approx 25 \text{ emu cm}^{-3}$ in Fig. 2(a)] in the AFM phase of the Fe-Rh layer [see Figs. S3(b) and S3(c) within the Supplemental Material for the $M(H)$ loops of an Fe-Rh(32) single layer [41]]. Figure 2(b) shows the temperature dependence of the magnetization, $M(T)$, at 1000 Oe near the magnetic phase transition of Fe-Rh. A sharp transition with a width of $\Delta T_{\text{FM-AFM}} \approx 30 \text{ K}$ is observed for the Fe(6)/Rh(2)/Fe-Rh(32) trilayer, which is consistent with the high S value. An Fe-Rh(32) single layer without an Fe layer also shows a sharp $\Delta T_{\text{FM-AFM}} (\approx 30 \text{ K})$ [see Fig. S5(a) within the Supplemental Material [41]]. The relatively broad transition ($\Delta T_{\text{FM-AFM}} \approx 50 \text{ K}$) for the Fe(6)/Fe-Rh(32) bilayer is likely to be due to an instability of the AFM phase induced by the magnetic exchange field and/or strain from the Fe layer [see Figs. S5(a)–S5(c)]

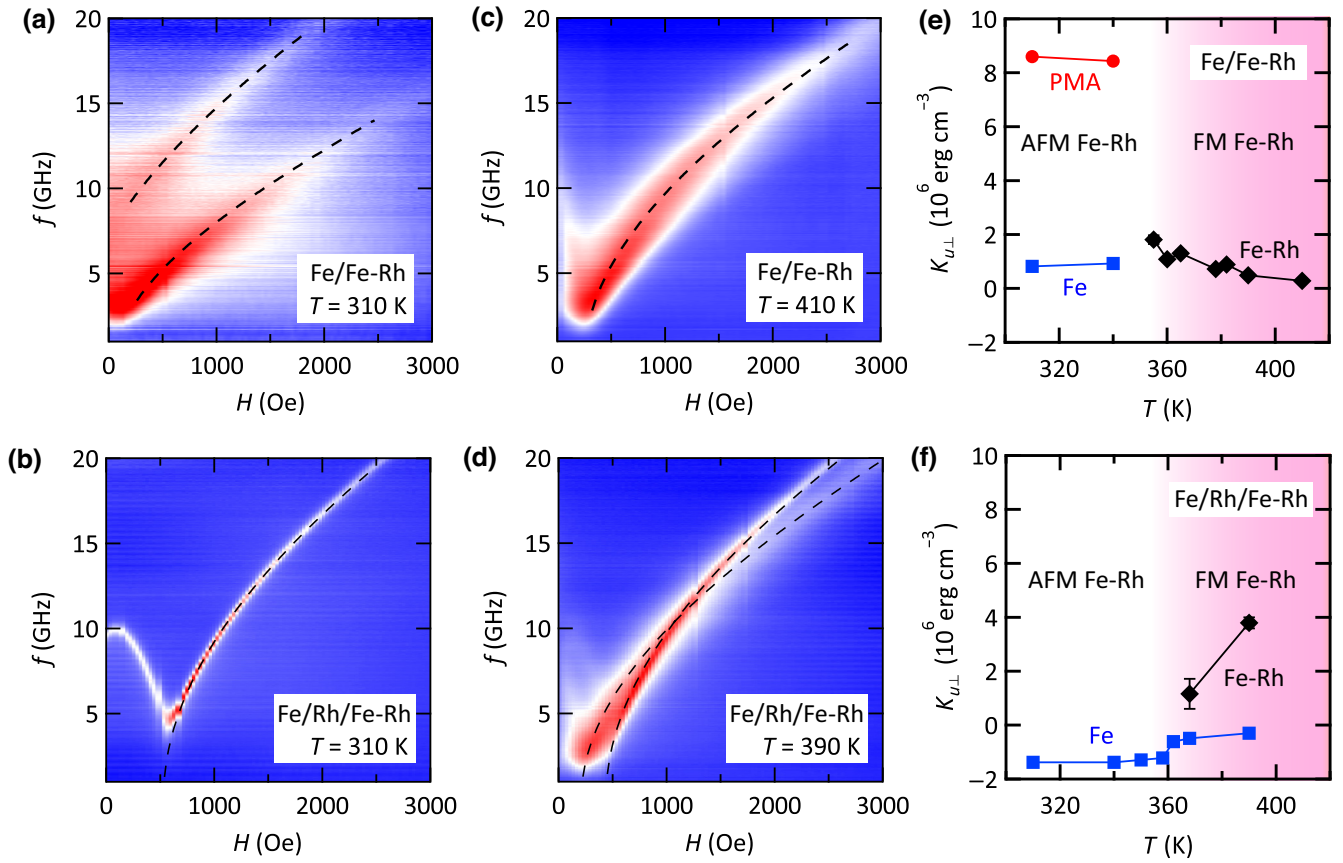


FIG. 3. Ferromagnetic resonance spectra for Fe(6 nm)/Fe-Rh(32 nm) at (a) 310 K and (c) 410 K, and Fe(6 nm)/Rh(2 nm)/Fe-Rh(32 nm) at (b) 310 K and (d) 390 K. Dashed curves represent least-squares regression-line fitting to the Kittel formula. Temperature dependence of the perpendicular-magnetic-anisotropy energy ($K_{u,\perp}$) estimated from the resonance spectra of (e) Fe(6 nm)/Fe-Rh(32 nm) and (f) Fe(6 nm)/Rh(2 nm)/Fe-Rh(32 nm).

within the Supplemental Material for the Fe-thickness dependence of $\Delta T_{\text{FM-AFM}}$ [41].

FMR spectra of the Fe(6)/Fe-Rh(32) bilayer and the Fe(6)/Rh(2)/Fe-Rh(32) trilayer at 310 K are shown in Figs. 3(a) and 3(b), respectively. The Fe(6)/Fe-Rh(32) bilayer shows two separate resonance curves [Fig. 3(a)] while the Fe(6)/Rh(2)/Fe-Rh(32) trilayer shows a single resonance curve [Fig. 3(b)]. This suggests the presence of an additional resonance mode originating from a magnetic exchange coupling at the Fe/Fe-Rh interface in the Fe(6)/Fe-Rh(32) bilayer. The comparable M_s values of the Fe(6)/Fe-Rh(32) bilayer and the Fe(6)/Rh(2)/Fe-Rh(32) trilayer [Fig. 2(a)] suggest that the exchange-coupled ferromagnetic layer giving the additional resonance mode is likely to exist within the Fe layer and an induced ferromagnetic moment within the Fe-Rh layer, as a result of magnetic proximity coupling, is negligibly small. From the Fe-thickness dependence of the resonance intensity [see Fig. S6(g) within the Supplemental Material [41]], we confirm that the resonance at lower frequency originates from the exchange-coupled Fe layer and the higher frequency originates from the

rest of the Fe layer. The resonance at lower frequency is stronger than that at higher frequency, indicating that the exchange-coupled Fe layer is dominant in the 6-nm-thick Fe layer. The resonance curves can be described by the Kittel formula for a thin film [43,44]: $f^2 = (1/2\pi)^2 (ge/2mc)^2 [4\pi M_s - (2K_{u,\perp}/M_s) + H + H_k](H + H_k)$, where g is the Landé g factor, e is the elementary charge, m is the electron mass, c is the speed of light, H_k is the in-plane anisotropy field, and $K_{u,\perp}$ is the perpendicular magnetic anisotropy energy. From a least-squares regression-line fitting [see dashed curves in Fig. 3(a)], we estimate $K_{u,\perp} = (8.6 \pm 0.1) \times 10^3 \text{ kerg cm}^{-3}$ and $H_k = -(8.1 \pm 0.9) \times 10 \text{ Oe}$ for the exchange-coupled Fe layer, and $K_{u,\perp} = (8.2 \pm 0.7) \times 10^2 \text{ kerg cm}^{-3}$ and $H_k = (3.4 \pm 0.1) \times 10^2 \text{ Oe}$ for the rest of the Fe layer, suggesting that the shift of the resonance frequency results from a notably large PMA of the exchange-coupled Fe layer. Since M_s of the Fe(6)/Fe-Rh(32) bilayer is comparable to that of the Fe(6)/Rh(2)/Fe-Rh(32) trilayer [see Fig. 2(a)], M_s of the exchange-coupled layer and the rest of the Fe layer should be comparable in the Fe(6)/Fe-Rh(32) bilayer, and hence, we use $M_s = 1.5 \times 10^3 \text{ emu cm}^{-3}$ (the

value from the VSM measurements) and $g = 2.09$ (a typical value for an Fe thin film [45–47]) for both the exchange-coupled layer and the rest of the Fe layer to estimate their H_k and $K_{u\perp}$ values.

Following a temperature increase up to 410 K, the Fe-Rh layer becomes ferromagnetic, leading to an overlapping of the two resonance curves in the Fe(6)/Fe-Rh(32) bilayer [Fig. 3(c)], suggesting that the Fe layer is entirely exchange coupled with the FM phase of the Fe-Rh layer. This is in contrast to the Fe(6)/Rh(2)/Fe-Rh(32) trilayer, in which magnetically decoupled Fe and Fe-Rh show two separate resonance curves [Fig. 3(d)]. Fitting the resonance curve of the Fe(6)/Fe-Rh(32) bilayer at 410 K to the Kittel formula yields $K_{u\perp} = (2.8 \pm 0.8) \times 10^2$ kerg cm⁻³ and $H_k = -(2.6 \pm 0.1) \times 10^2$ Oe, where we use $M_s = 1.2 \times 10^3$ emu cm⁻³ obtained from the VSM measurement [see Fig. S3(c) within the Supplemental Material [41]] and $g = 2.05$ [a typical value for an Fe-Rh epitaxial film on a MgO(001) substrate [48]]. $K_{u\perp}$ at 410 K is more than an order of magnitude smaller than that of the exchange-coupled layer at 310 K, indicating that the large PMA at the Fe/Fe-Rh interface disappears following the appearance of the FM phase in Fe-Rh. Hence, PMA is controllable by the magnetic phase transition of Fe-Rh.

In Fig 3(e), we plot the temperature dependence of $K_{u\perp}$ estimated from the FMR curves of the Fe(6)/Fe-Rh(32) bilayer. Notably different $K_{u\perp}$ values are obtained from the two different FMR modes below 340 K. The emergence of the FM phase of Fe-Rh following a temperature increase leads to a sudden disappearance of the large $K_{u\perp}$. The $K_{u\perp}$ values of the Fe(6)/Rh(2)/Fe-Rh(32) trilayer show a different trend [Fig. 3(f)]. The Fe layer shows small $K_{u\perp}$ values (in-plane magnetic anisotropy) over the whole temperature range investigated, suggesting that the Fe layer is magnetically decoupled from Fe-Rh. The two different $K_{u\perp}$ values from the separate FMR modes of the Fe and Fe-Rh above 340 K also suggests the absence of exchange coupling between Fe and Fe-Rh [see Figs. S7 and S8 within the Supplemental Material for the temperature dependence of the FMR spectra for the Fe(6)/Fe-Rh(32) bilayer and the Fe(6)/Rh(2)/Fe-Rh(32) trilayer [41]].

An AFM-induced PMA at a FM-AFM interface is reported in limited systems, such as Ni/CoO [10] and Fe/Mn [12]. We note that our [001]-oriented Fe-Rh films grown on a MgO (001) substrate should have a compensated AFM spin order at the Fe/Fe-Rh interface, and therefore, the exchange-bias effect is absent, similar to the Fe/Mn case [12]. The compensated AFM spin order can cause spin frustration at the FM-AFM interface and a noncollinear exchange coupling can be established to minimize the interface-exchange energy, which forces interfacial spins to align perpendicular to the interface [11,49,50]. At the Fe/Mn interface, the noncollinear exchange coupling stabilizing PMA is mediated by unpinned Mn spins

within a unit cell of Mn from the interface [12]. Although the moment of such unpinned spins is small and hard to detect [12,51], they are observable as an enhancement of H_c of the adjacent FM layer [12,51], which is consistent with the magnetization properties of our Fe/Fe-Rh bilayer. Furthermore, the disappearance of the large PMA, following the AFM-to-FM transition of Fe-Rh observed in this work, is consistent with the Fe/Mn system in which decreasing Mn thickness results in a reduction of PMA due to reduced AFM order [12].

IV. CONCLUSION

In conclusion, we demonstrate a large PMA induced at an Fe/Fe-Rh interface from FMR measurements. PMA disappears following the magnetic phase transition of Fe-Rh from the AFM to the FM state, suggesting that a magnetic exchange coupling between the FM order of Fe and the AFM order of Fe-Rh is necessary to develop PMA. Although further study is needed to clarify the exact mechanism(s), the large PMA, in conjunction with its controllability through the magnetic phase transition, demonstrated in this work can provide a platform for controlling high-density spintronic devices.

ACKNOWLEDGMENTS

This work is supported by JST CREST (Grant No. JPMJCR18J); JSPS KAKENHI (Grants No. 21H04614 and No. 20K23374); JST FOREST (Grant No. JPMJFR212V), JSPS Bilateral Joint Research Projects (Grant No. JPJSBP120197716); and Advanced Research Infrastructure for Materials and Nanotechnology in Japan (ARIM) of the Ministry of Education, Culture, Sports, Science and Technology (MEXT) (Proposal No. JPMXP1222NU0063).

-
- [1] D. Weller and A. Moser, Thermal effect limits in ultrahigh-density magnetic recording, *IEEE Trans. Magn.* **35**, 4423 (1999).
 - [2] S. Mangin, D. Ravelosona, J. A. Katine, M. J. Carey, B. D. Terris, and E. E. Fullerton, Current-induced magnetization reversal in nanopillars with perpendicular anisotropy, *Nat. Mater.* **5**, 210 (2006).
 - [3] N. Nakajima, T. Koide, T. Shidara, H. Miyauchi, H. Fukutani, A. Fujimori, K. Iio, T. Katayama, M. Nývlt, and Y. Suzuki, Perpendicular Magnetic Anisotropy Caused by Interfacial Hybridization via Enhanced Orbital Moment in Co/Pt Multilayers: Magnetic Circular X-Ray Dichroism Study, *Phys. Rev. Lett.* **81**, 5229 (1998).
 - [4] D. Weller, Y. Wu, J. Stohr, M. G. Samant, B. D. Hermsmeier, and C. Chappert, Orbital magnetic moments of Co in multilayers with perpendicular magnetic anisotropy, *Phys. Rev. B* **49**, 888 (1994).

- [5] J. Hayakawa, S. Ikeda, Y. M. Lee, R. Sasaki, T. Meguro, F. Matsukura, H. Takahashi, and H. Ohno, Current-driven magnetization switching in CoFeB/MgO/CoFeB magnetic tunnel junctions, *Jpn. J. Appl. Phys.* **44**, L1267 (2005).
- [6] S. Ikeda, K. Miura, H. Yamamoto, K. Mizunuma, H. D. Gan, M. Endo, S. Kanai, J. Hayakawa, F. Matsukura, and H. Ohno, A perpendicular-anisotropy CoFeB-MgO magnetic tunnel junction, *Nat. Mater.* **9**, 721 (2010).
- [7] J. W. Koo, S. Mitani, T. T. Sasaki, H. Sukegawa, Z. C. Wen, T. Ohkubo, T. Niizeki, K. Inomata, and K. Hono, Large perpendicular magnetic anisotropy at Fe/MgO interface, *Appl. Phys. Lett.* **103**, 192401 (2013).
- [8] T. Devolder, P. H. Ducrot, J. P. Adam, I. Barisic, N. Vernier, J. Von Kim, B. Ockert, and D. Ravelosona, Damping of $\text{Co}_x\text{Fe}_{80-x}\text{B}_2\text{O}$ ultrathin films with perpendicular magnetic anisotropy, *Appl. Phys. Lett.* **102**, 022407 (2013).
- [9] J. Okabayashi, J. W. Koo, H. Sukegawa, S. Mitani, Y. Takagi, and T. Yokoyama, Perpendicular magnetic anisotropy at the interface between ultrathin Fe film and MgO studied by angular-dependent x-ray magnetic circular dichroism, *Appl. Phys. Lett.* **105**, 122408 (2014).
- [10] P. Kuświk, P. L. Gastelois, M. M. Soares, H. C. N. Tolentino, M. De Santis, A. Y. Ramos, A. D. Lamirand, M. Przybylski, and J. Kirschner, Effect of CoO/Ni orthogonal exchange coupling on perpendicular anisotropy of Ni films on Pd(001), *Phys. Rev. B* **91**, 134413 (2015).
- [11] B. Y. Wang, N. Y. Jih, W. C. Lin, C. H. Chuang, P. J. Hsu, C. W. Peng, Y. C. Yeh, Y. L. Chan, D. H. Wei, W. C. Chiang, and M. T. Lin, Driving magnetization perpendicular by antiferromagnetic-ferromagnetic exchange coupling, *Phys. Rev. B* **83**, 104417 (2011).
- [12] B. Wang, J. Hong, K. O. Yang, Y. Chan, D. Wei, H. Lin, and M. Lin, How Antiferromagnetism Drives the Magnetization of a Ferromagnetic Thin Film to Align Out of Plane, *Phys. Rev. Lett.* **110**, 117203 (2013).
- [13] B. Y. Wang, M. S. Tsai, C. W. Huang, C. W. Shih, C. J. Chen, K. Lin, J. J. Li, N. Y. Jih, C. I. Lu, T. H. Chuang, and D. H. Wei, Effects of the antiferromagnetic spin structure on antiferromagnetically induced perpendicular magnetic anisotropy, *Phys. Rev. B* **96**, 094416 (2017).
- [14] B. Y. Wang, P. H. Lin, M. S. Tsai, C. W. Shih, M. J. Lee, C. W. Huang, N. Y. Jih, P. Y. Cheng, and D. H. Wei, Crucial role of interlayer distance for antiferromagnet-induced perpendicular magnetic anisotropy, *Phys. Rev. B* **92**, 214435 (2015).
- [15] M. Fallot and R. Hocart, Sur l'apparition du ferromagnétisme par élévation de température dans des alliages de fer et de rhodium, *Rev. Sci.* **77**, 498 (1939).
- [16] L. Muldewar and F. de Bergevin, Antiferromagnetic-ferromagnetic transformation in FeRh, *J. Chem. Phys.* **35**, 1904 (1961).
- [17] J. S. Kouvel and C. C. Hartelius, Anomalous magnetic moments and transformations in the ordered alloy FeRh, *J. Appl. Phys.* **33**, 1343 (1962).
- [18] C. J. Schinkel, R. Hartog, and F. H. A. M. Hochstetbach, On the magnetic and electrical properties of nearly equiatomic ordered FeRh alloys, *J. Phys. F: Met. Phys.* **4**, 1412 (1974).
- [19] J.-U. Thiele, S. Maat, and E. E. Fullerton, FeRh/FePt exchange spring films for thermally assisted magnetic recording media, *Appl. Phys. Lett.* **82**, 2859 (2003).
- [20] N. T. Nam, W. Lu, and T. Suzuki, Exchange bias of ferromagnetic/antiferromagnetic in FePt/FeRh bilayers, *J. Appl. Phys.* **105**, 07D708 (2009).
- [21] I. Suzuki, Y. Hamasaki, M. Itoh, and T. Taniyama, Controllable exchange bias in Fe/metamagnetic FeRh bilayers, *Appl. Phys. Lett.* **105**, 172401 (2014).
- [22] P. Drózdź, M. Ślęzak, K. Matlak, B. Matlak, K. Freindl, D. Wilgocka-Ślęzak, N. Spiridis, J. Korecki, and T. Ślęzak, Switching of Co Magnetization Driven by Antiferromagnetic-Ferromagnetic Phase Transition of FeRh Alloy in Co/FeRh Bilayers, *Phys. Rev. Appl.* **9**, 034030 (2018).
- [23] R. O. Cherifi, V. Ivanovskaya, L. C. Phillips, A. Zobelli, I. C. Infante, E. Jacquet, V. Garcia, S. Fusil, P. R. Briddon, N. Guiblin, A. Mougin, A. A. Ünal, F. Kronast, S. Valencia, B. Dkhil, A. Barthélémy, and M. Bibes, Electric-field control of magnetic order above room temperature, *Nat. Mater.* **13**, 345 (2014).
- [24] I. Fina, A. Quintana, X. Martí, F. Sánchez, M. Foerster, L. Aballe, J. Sort, and J. Fontcuberta, Reversible and magnetically unassisted voltage-driven switching of magnetization in FeRh/PMN-PT, *Appl. Phys. Lett.* **113**, 152901 (2018).
- [25] I. Suzuki, M. Itoh, and T. Taniyama, Elastically controlled magnetic phase heterostructure, *Appl. Phys. Lett.* **104**, 022401 (2014).
- [26] P. H. L. Walter, Exchange inversion in ternary modifications of iron rhodium, *J. Appl. Phys.* **35**, 938 (1964).
- [27] H. Miyajima, S. Yuasa, and Y. Otani, First-order magnetic phase transitions observed in bct FeRh–Pt, Pd systems, *Jpn. J. Appl. Phys.* **32**, 232 (1993).
- [28] S. Yuasa, H. Miyajima, and Y. Otani, Magneto-volume and tetragonal elongation effects on magnetic phase transitions of body-centered tetragonal FeRh_{1-x}Pt_x, *J. Phys. Soc. Jpn.* **63**, 3129 (1994).
- [29] T. Maruyama, Y. Shiota, T. Nozaki, K. Ohta, N. Toda, M. Mizuguchi, A. A. Tulapurkar, T. Shinjo, M. Shiraiishi, S. Mizukami, Y. Ando, and Y. Suzuki, Large voltage-induced magnetic anisotropy change in a few atomic layers of iron, *Nat. Nanotechnol.* **4**, 158 (2009).
- [30] M. Endo, S. Kanai, S. Ikeda, F. Matsukura, and H. Ohno, Electric-field effects on thickness dependent magnetic anisotropy of sputtered MgO/Co₄₀Fe₄₀B₂₀/Ta structures, *Appl. Phys. Lett.* **96**, 212503 (2012).
- [31] W. Wang, M. Li, S. Hageman, and C. L. Chien, Electric-field-assisted switching in magnetic tunnel junctions, *Nat. Mater.* **11**, 64 (2012).
- [32] G. Yu, Z. Wang, M. Abolfath-beygi, C. He, X. Li, I. A. Alhomoudi, P. K. Amiri, and K. L. Wang, Strain-induced modulation of perpendicular magnetic anisotropy in Ta/CoFeB/MgO structures investigated by ferromagnetic resonance, *Appl. Phys. Lett.* **106**, 072402 (2015).
- [33] U. Bauer, L. Yao, A. J. Tan, P. Agrawal, S. Emori, H. L. Tuller, S. Van Dijken, and G. S. D. Beach, Magneto-ionic control of interfacial magnetism, *Nat. Mater.* **14**, 174 (2015).

- [34] A. J. Schellekens, A. Van Den Brink, J. H. Franken, H. J. M. Swagten, and B. Koopmans, Electric-field control of domain wall motion, *Nat. Commun.* **3**, 847 (2012).
- [35] W. Lin, N. Vernier, G. Agnus, K. Garcia, B. Ocker, W. Zhao, E. E. Fullerton, and D. Ravelosona, Universal domain wall dynamics under electric field in Ta/CoFeB/MgO devices with perpendicular anisotropy, *Nat. Commun.* **7**, 13532 (2016).
- [36] K. L. Wang, H. Lee, and P. Khalili Amiri, Magnetolectric random access memory-based circuit design by using voltage-controlled magnetic anisotropy in magnetic tunnel junctions, *IEEE Trans. Nanotechnol.* **14**, 992 (2015).
- [37] M. A. de Vries, M. Loving, A. P. Mihai, L. H. Lewis, D. Heiman, and C. H. Marrows, Hall-effect characterization of the metamagnetic transition in FeRh Hall-effect characterization of the metamagnetic transition in FeRh, *New J. Phys.* **15**, 013008 (2013).
- [38] T. Miyanaga, T. Itoga, T. Okazaki, and K. Nitta, Local structural change under antiferro- and ferromagnetic transition in FeRh alloy, *J. Phys. Conf. Ser.* **190**, 012097 (2009).
- [39] T. Usami, M. Itoh, and T. Taniyama, Temperature dependence of the effective Gilbert damping constant of FeRh thin films, *AIP Adv.* **11**, 045302 (2021).
- [40] I. Suzuki, T. Koike, M. Itoh, and T. Taniyama, Stability of ferromagnetic state of epitaxially grown ordered FeRh thin films, *J. Appl. Phys.* **105**, 07E501 (2009).
- [41] See the Supplemental Material at <http://link.aps.org/supplemental/10.1103/PhysRevApplied.19.064077> for detailed structural and magnetic characterization.
- [42] S. Yuasa, M. Nývlt, and T. Katayama, Exchange coupling of NiFe/FeRh–Ir thin films, *J. Appl. Phys.* **83**, 6813 (1998).
- [43] J. P. Nibarger, R. Lopusnik, Z. Celinski, and T. J. Silva, Variation of magnetization and the Landé g factor with thickness in Ni-Fe films, *Appl. Phys. Lett.* **83**, 93 (2003).
- [44] H. Mizuno, T. Moriyama, M. Kawaguchi, M. Nagata, K. Tanaka, T. Koyama, D. Chiba, and T. Ono, Ferromagnetic resonance measurements in sub-nanometer Fe films, *Appl. Phys. Express* **8**, 073003 (2015).
- [45] O. Hitoshi, I. Seisaku, M. Mitsuhiro, and K. Eiji, Magnetic anisotropies of Fe/MgO multilayers determined by submillimeter wave FMR, *J. Phys. Soc. Jpn.* **62**, 4467 (1993).
- [46] Y. V. Goryunov, N. N. Garif'yanov, G. G. Khaliullin, and I. A. Garifullin, Magnetic anisotropies of sputtered Fe films on MgO substrates, *Phys. Rev. B* **52**, 13450 (1995).
- [47] *Numerical Data and Functional Relationships in Science and Technology, Landolt-Bornstein, New Series*, Vol. III/1 (Springer, Heidelberg, 1986).
- [48] E. Mancini, F. Pressacco, M. Haertinger, E. E. Fullerton, T. Suzuki, G. Woltersdorf, and C. H. Back, Magnetic phase transition in iron–rhodium thin films probed by ferromagnetic resonance, *J. Phys. D: Appl. Phys.* **46**, 245302 (2013).
- [49] B. Wang, C.-C. Chiu, and W.-C. Lin, Enhanced perpendicular magnetic anisotropy in Fe/Mn bilayers by incorporating ultrathin ferromagnetic underlayer through magnetic proximity effect, *Appl. Phys. Lett.* **103**, 042407 (2013).
- [50] Y. Y. Wang, C. Song, G. Y. Wang, F. Zeng, and F. Pan, Evidence for asymmetric rotation of spins in antiferromagnetic exchange-spring, *New J. Phys.* **16**, 123032 (2014).
- [51] B. Y. Wang, C. H. Chuang, S. S. Wong, J. J. Chiou, W. C. Lin, Y. L. Chan, D. H. Wei, and M. Lin, Flipping magnetization induced by noncollinear ferromagnetic-antiferromagnetic exchange coupling, *Phys. Rev. B* **85**, 094412 (2012).